Available online at www.sciencedirect.com
ScienceDirect
Ceramics International 37 (2011) 2869–2877
CERAMICS INTERNATIONAL
www.elsevier.com/locate/ceramint

Dip-coating of 8YSZ nanopowder for SOFC applications

Hanna Tikkanen [a,b,*], Crina Suciu [b], Ivar Wærnhus [b], Alex C. Hoffmann [a,b]

[a] University of Bergen, Institution of Physics and Technology, Allégaten 55, NO-5007 Bergen, Norway
[b] Prototech AS, Fantoftveien 38, NO-5075 Bergen, Norway

Received 23 March 2011; received in revised form 29 April 2011; accepted 2 May 2011
Available online 11 May 2011

Abstract

A dip-coating method was used to obtain 8YSZ thin films formed from nanoparticles on anode support for SOFC applications. 8YSZ nanopowder was obtained via a modified sol–gel method using sucrose and pectin as organic precursors. The nanoparticles were suspended in ethanol using phosphate ester (PE) and polyvinyl butyral (PVB) as dispersant and binder, respectively. The microstructure of the sintered films were analyzed with SEM. The suspension preparation conditions were tuned in order to achieve high initial green density of the 8YSZ films subsequently determining the final sintered microstructure. In addition, the effect of the linear shrinkage of the anode substrate on the 8YSZ film microstructure was studied.

Keywords: A. Films; E. Fuel cells; Sol–gel; Nanoparticles; Dip-coating

1. Introduction

Yttria-stabilized zirconia (YSZ) is the most common electrolyte used in solid oxide fuel cells (SOFCs) [1]. Zirconia doped with 8 mol% of yttria (8YSZ) with cubic structure is found to have the highest ionic conductivity in the group of yttria-stabilized zirconia electrolytes [2].

There are still many challenges that need to be solved before a wide commercialization of fuel cell technology can take place. The high operating temperature (800–1000 °C) limits the choice of suitable materials and the current trend is to lower the operating temperature to 600–800 °C [1]. However, at these temperatures the oxide ion conductivity of the electrolyte drops drastically [2]. The resistivity of the electrolyte can be decreased by reducing its thickness. Because of the low mechanical strength of thin electrolyte films made of 8YSZ, the reduction of thickness is difficult to achieve in the electrolyte-supported configuration [3]. The electrode-supported configuration can be used in this case with the anode-supported cell being favoured over cathode-supported cell due to the high sintering temperature of the 8YSZ. At the typical sintering temperature of the 8YSZ the cathode might become too dense and/or highly resistant reaction products form at the interface between the cathode and the electrolyte in the co-sintering process [1,4–6].

Thin electrolyte layers can be manufactured in many ways including physical vapor deposition (PVD), such as sputtering [7], chemical vapor deposition (CVD) [8], plasma technologies [9] and electrophoretic deposition (EPD) [4–6,10–12]. Dip-coating is a cost-effective wet-chemical method which has been used widely in the literature to obtain thin layers [13–22]. In dip-coating a porous substrate is immersed in a liquid in which the particles to be deposited are suspended. Due to the capillary action of the pores, the liquid fills the pores leaving a coating on the substrate surface [13].

Reducing the particle size to nanoscale of the precursor powder for SOFC components may be advantageous. Using nanopowders as precursors for the manufacture of SOFC electrodes have been demonstrated to enhance the triple phase boundary and thereby improving the performance of anode-supported cells [16,21]. Sintering of nanograined particles may take place at lower temperatures [10,22–24], which is interesting for both the electrolyte and the electrode-supported configurations. In addition to processing considerations, lowering the sintering temperature decreases the grain size of the particles. Smaller grain size is claimed by some to lead to the formation of narrower grain boundaries. There are indications that narrower grain boundaries result in higher

* Corresponding author at: Prototech AS, Fantoftveien 38 NO-5075 Bergen, Norway. Tel.: +47 94 14 03 46; fax: +47 56 57 41 14.
E-mail addresses: hanna.tikkanen@prototech.no, hanna-mari.tikkanen@ift.uib.no (H. Tikkanen).

0272-8842/$36.00
doi:10.1016/j.ceramint.2011.05.006

ionic conductivity [25]. A study by Wang et al. on dip-coating of commercial YSZ particles on anode-supported cell indicated that the smaller grain size of YSZ induced by a lowering in the sintering temperature enhanced the conductivity of the YSZ electrolyte [20]. In the same study, the measured electrochemical characteristics of the cell implied that a low-temperature sintering process improved the anode performance.

For SOFC application gas-tight and dense electrolytes with homogeneous microstructure are important. The drawbacks common to all wet-chemical coating methods, which are, among other things, cracking of the coating during drying and/or sintering have been discussed by several authors [10–14,18–20,26]. In general by careful adjustment of the chemistry of the suspension by using additives [11,12,27], by a judicious choice of solvents [26] or by humidity control [14] cracking during drying can be avoided. A common practice to avoid cracking during co-sintering is by using substrates that shrink together with the coating [10,22,26,28]. Substrate shrinkage during co-sintering is also reported to aid the densification of the coating [17,19,22,29].

Using nanosized particles for dip-coating raises also some challenges; during post-synthesis treatment they have a high tendency to agglomerate due to their large surface area. The state of agglomeration of ceramic particles dictates the sintering behaviour and thus the final microstructure [6,10,14,22,24,30,31]. Agglomeration of particles leads to a low packing density of the green film and subsequently to a poor densification of the final film after sintering. Dispersion of nanoparticles have been achieved by charging of the particles preventing the particles coming together by electrostatic repulsion [6,10] or by additives providing steric hindrance [22]. Formed agglomerates can also be broken down mechanically by using ultrasound [6,10,24] or/and ball-milling [10,22,30,31].

In this work, 8YSZ nanopowder was obtained by a modified sol–gel method using sucrose and pectin as organic precursors. Sucrose and pectin form an organic matrix where the metal cations are trapped stopping the growth of the particles at nanoscale. The organic precursors also function as internal fuel giving rise to homogeneous and weakly-agglomerated nanoparticles. In previous work by some of the present authors the effect of different synthesis parameters of the modified sol–gel method on the powder characteristics have been investigated for YSZ [32,33]. The sintering properties of the electrolyte pellets formed from YSZ nanopowder and the ionic conductivity of the resulting materials have been studied [31]. The present study takes the next step to prepare SOFC half-cells by dip-coating 8YSZ nanosized particles on porous NiO–YSZ anode substrates. The preparation conditions for obtaining fully dense electrolyte films using commercial 8YSZ powder was tested first and then these results were used as the starting point for obtaining thin films with nanopowder suspensions. The presented work consists of two parts: (1) the effect of the suspension preparation parameters on the microstructure of the electrolyte film, and (2) the pre-sintering condition of the anode substrate on the final film microstructure.

Table 1
The starting compounds.

$ZrCl_4$ (g)	$Y(NO_3)_3{\cdot}6H_2O$ (g)	Sugar (g)	Pectin (g)	H_2O (ml)
8.1557	2.3314	50	5	400

2. Experiments

2.1. Preparation of the 8YSZ nanopowder

The 8YSZ nanoparticles were obtained by a modified sol–gel method. Zirconium tetracloride ($ZrCl_4$, 99.5+%, Aldrich) and yttrium nitrate ($Y(NO_3)_3{\cdot}6H_2O$, 99.9%, Aldrich) were used as starting material. The appropriate quantities to obtain 8 mol% of yttria-stabilized zirconia was calculated and used. The amounts of starting compounds are presented in Table 1. The weighted starting compounds were dissolved in deionized water under magnetic stirring. The clear solutions were then transferred to alumina dishes and set on a sand bath. Sucrose and pectin were added to the solutions in a ratio of 50:5. The solvent was gradually evaporated in order to form the gel. The final dry gel was then calcined at a temperature of 1000 °C to form the 8YSZ nanoparticles. The calcination program applied had a heating plateau at 600 °C for 1 h to burn of the organic material in the gel. Thermal analysis (TGA) of the calcination process of the dried gel can be found in previous work [33]; during that work the exothermic burnout of organic components was identified, and this information has been used in designing the calcination scheme. A schematic presentation of the procedure to obtain the nanopowder is presented in Fig. 1.

The obtained 8YSZ nanoparticles were characterized using transmission electron microscopy (TEM), X-ray diffraction (XRD) and Brunauer, Emmet and Teller adsorption (BET).

2.2. Preparation of the porous NiO–YSZ substrate

The powders used in the present work are NiO–YSZ formed by calcining two oxide powders NiO (Nickel (II) Oxide black,

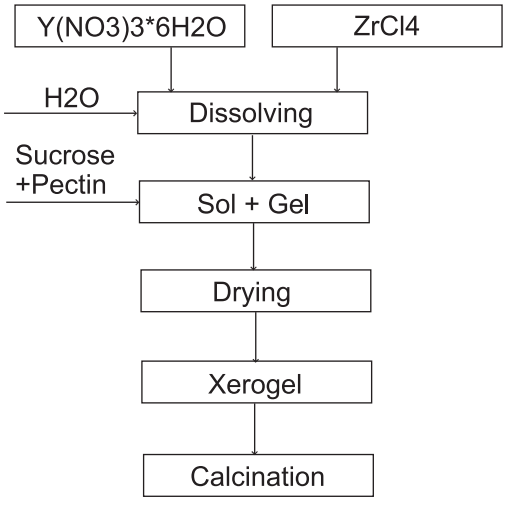

Fig. 1. Schematic presentation of obtaining the 8YSZ nanopowder.

Ni 76%, Alfa Aesar) and 8YSZ (TZ-8Y, Tosoh). The NiO was calcined at 700 °C and 28 g of the powder was ball-milled with zirconia balls in deionized water for 24 h. Then 11 g of calcined (at 1100 °C) 8YSZ and 11 g of uncalcined 8YSZ were added and the milling process was continued for another 24 h. The powder was then set to dry. The dried powder was then mortered, sieved and pressed to pellets (d = 20 mm) using a uniaxial press (1200 psi = 8.3 MPa). In order to add mechanical strenght to the substrate for further processing, the pressed substrates were presintered. Various temperatures were used for the presintering (1000, 1100, 1200 and 1300 °C) with a heating rate of 200 °C/h and a dwell time of 2 h.

2.3. Dip-coating

The commercial 8YSZ suspension was prepared by mixing 10 g of 8YSZ (TZ-8Y, Tosoh), 0.15 g of phosphate ester dispersant (PE, PE105, AKZO NOBEL) and 0.3 g of polyvinyl butyral binder (PVB, B-98 Lot # T44499, Tape Casting Warehouse) with 100 ml ethanol (technical ethanol, KEMETYL). The suspension was ultrasonically treated for 1 h.

The suspensions for dip-coating of the 8YSZ nanopowder were prepared by using three different procedures. The first set was prepared in manner identical to that for the commercial suspension. The second set was prepared by mixing 10 g of in-house produced 8YSZ and 0.15 g of PE with 100 ml ethanol. The suspension was ball-milled for 24 h and then 0.3–0.8 g of PVB binder was added. After the addition of binder the suspension was ball-milled another 24 h. The suspension was then ultrasonically mixed for 1 h in an ultrasonic bath before deposition. The third procedure involved using suspensions from the second set and allowing them to settle for 24 h. The precipitated powder was then removed and the suspensions was ultrasonically treated for 1 h followed by dip-coating.

The electrolyte films were obtained by dip-coating the porous NiO–YSZ substrate in the suspension. Before dip-coating a piece of parchment paper was glued (Loctite 401) on one side of the substrate. This was done to expose one side only of the planar substrate to the 8YSZ suspension which was therefore only subject to deposition on the exposed substrate side. Both the parchment paper and the glue are burnt off during the co-sintering process. The porous substrate was then attached to a wire. The dip-coating bath was placed on a manual lab jack. The substrate was slowly withdrawn from the suspension by lowering the platform on which the suspension was standing. The applied dip-coating time was 30 s for both the commercial and nanopowder suspensions. A schematic representation of the dip-coating set-up is presented in Fig. 2.

The obtained green films were dried at room temperature. After drying the green electrolyte films were co-sintered with anode substrates using the following program: a heating rate of 40 °C/h to 600 °C with a dwell time of 1 h to burn of the organic material in the green 8YSZ film. A heating rate of 200 °C/h was applied to reach the final sintering temperature of 1400 °C. The dwell time at the top temperature was 2 h. The morphology of the sintered 8YSZ thin films was studied by scanning electron microscopy (SEM, Zeiss Supra 55VP).

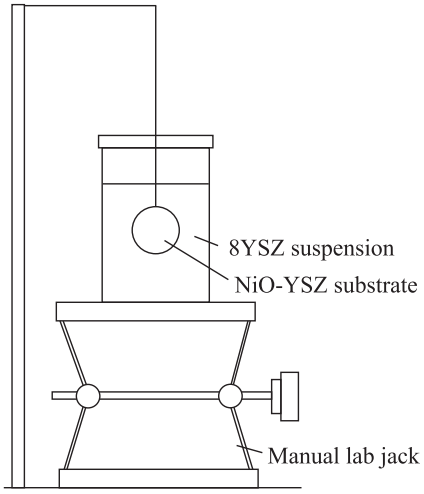

Fig. 2. Sketch of the dip-coating setup.

2.4. Sintering curves

The sintering curves of the green 8YSZ bodies and the NiO–YSZ substrates pre-sintered at different temperatures were studied by a dilatometer (L75V, Linseis). The anode samples for the dilatometer were pressed pellets (p = 1200 psi) which were cut to smaller pieces and then pre-sintered for 2 h at different temperatures (1000, 1100, 1200 and 1300 °C) with a heating rate of 200 °C/h. The 8YSZ green bodies were prepared by allowing the suspensions used for dip-coating to settle and removing the precipitated powder. The precipitated powder was then formed in a cylinder shape. The sintering curves of the samples was measured using the same sintering program as in the co-sintering step.

3. Results and discussion

3.1. Characterization of the in-house produced 8YSZ

Fig. 3 presents a TEM image (JEOL-JEM-1011) of the obtained calcined 8YSZ nanoparticles. The particle size was calculated by measuring 10 particles from the image. The average particle size was approximately 40 nm. Fig. 4 presents a TEM image of (JEOL-2100) the commercial 8YSZ powder showing clusters of size between 100 and 200 nm which agrees with the manufacturer specification.

Fig. 5 shows the X-ray spectrum of the 8YSZ powder calcined at 1000 °C. The X-ray diffraction measurements were carried out with Cu K-α radiation on a Bruker diffractometer under angles ranging from 20° to 100° with a step size of 0.02° and a counting rate of 3 s per scanning step. The spectrum shows the presence of one phase: YSZ, in the Fm - $3m$ cubic type structure. There is no indication of other phases present. The mean crystallite size can be calculated from the full width at half maximum (FWHM) from the obtained diffraction pattern. For particles calcinated at 1000 °C the crystallite size was calculated to be 20 nm.

BET adsorption analysis was used to measure the specific surface area of the synthesized nanoparticles. The BET

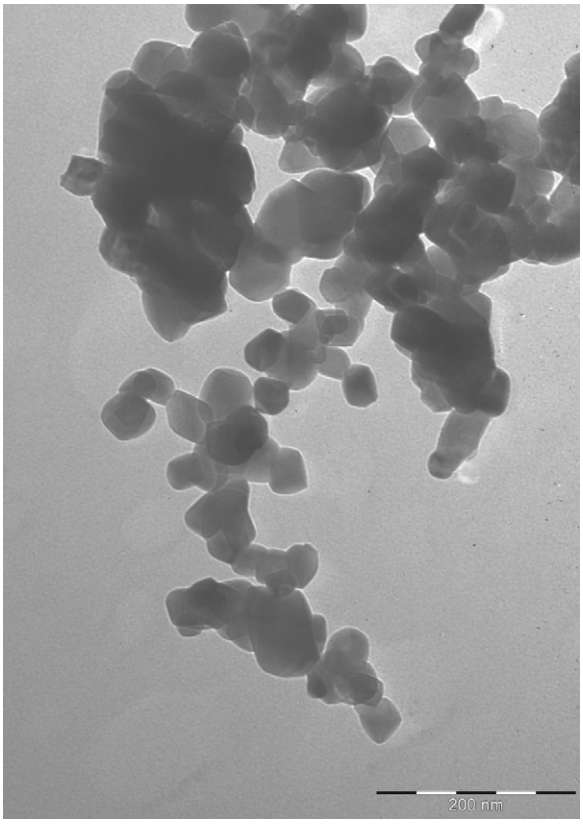

Fig. 3. TEM image of the 8YSZ powder calcinated at 1000 °C for 2 h.

measurements were carried out using a Gemini 2380 from Micromeritics. The samples were heated to 300 °C and degassed for 3 h under vacuum before the analysis. The singlepoint and multipoint specific surface area were approximately 24 and 25 $m^2\ g^{-1}$, respectively. Assuming the particles to be spherical and using a density, ρ, of 5960 $kg\ m^{-3}$, the

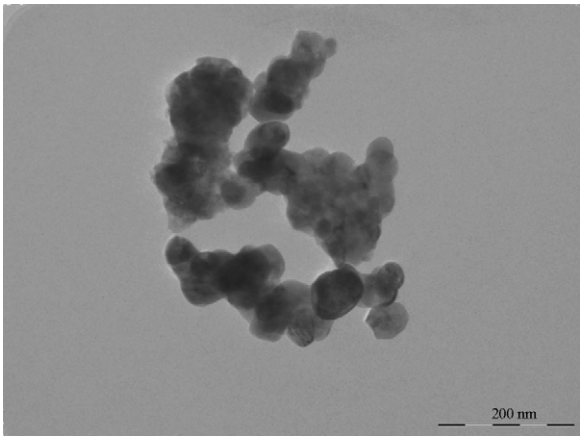

Fig. 4. TEM image of the commercial sub-micronsize 8YSZ powder.

Sauter mean diameter of the particles, d, can be estimated from the specific surface area, *ssa*, by the following equation:

$$ssa = \frac{6}{d\,\rho} \quad (1)$$

By inserting the values for the density and specific surface area (multipoint *ssa*), Eq. (1) gives a mean diameter of the 8YSZ nanoparticles of approximately 40 nm, which is in good agreement with the TEM results.

3.2. Sintering characteristics of 8YSZ electrolyte and NiO–YSZ anode

It is important to control the co-sintering process. Ceramic materials typically undergo dimensional changes during sintering [23,26]. The different components should be prepared in such a way that the total shrinkage of the components match each other. A mismatch in the shrinkage would produce stress

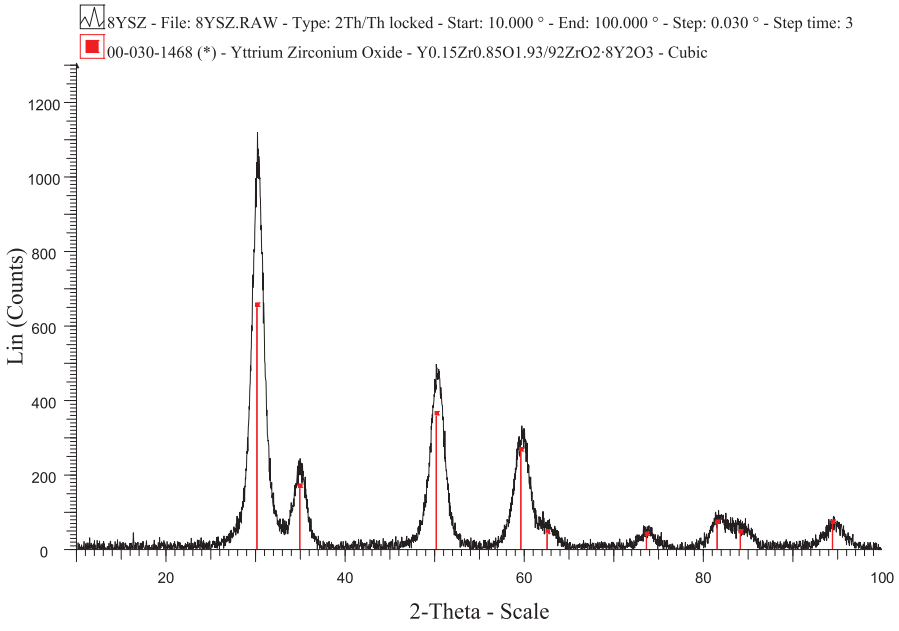

Fig. 5. XRD pattern of the 8YSZ powder calcinated at 1000 °C for 2 h.

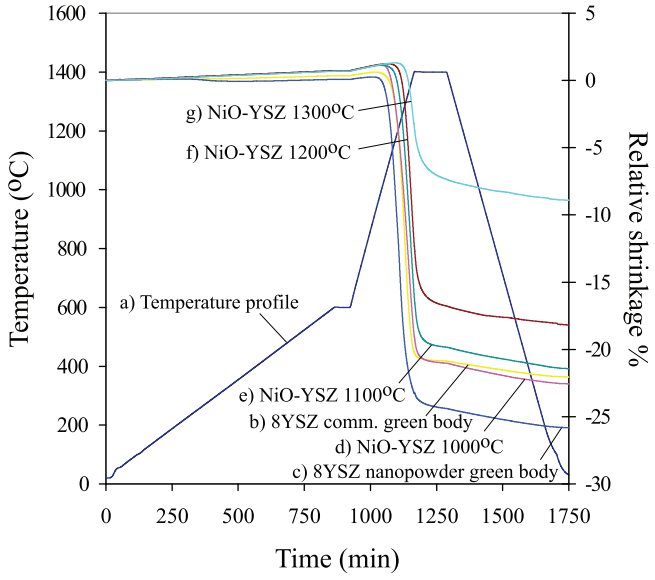

Fig. 6. (a) Temperature profile and the shrinkage behaviour of (b) 8YSZ commercial green body, (c) 8YSZ green nanopowder, (d) NiO–YSZ pre-sintered at 1000 °C, (e) NiO–YSZ pre-sintered at 1100 °C, (f) NiO–YSZ pre-sintered at 1200 °C and (g) NiO–YSZ pre-sintered at 1300 °C.

which can lead to cracking of the electrolyte film during the co-sintering process [10,22,28]. As already mentioned in the introduction, the linear shrinkage of the anode-support also affects the densification of the electrolyte film [17,19,22,29]. Some example values for shrinkage found in the literature are: Substrate shrinkage of above 15% has been found to produce fully densified GDC electrolyte films under single dipping conditions [17]. Tubular anode support shrinkage of ∼20% has been found sufficient to produce fully densified YSZ layers [19]. Linear shrinkage of 22% has been found to produce densified microstructure of YSZ films obtained by EPD on anode substrates [29]. Since there is probably no universal threshold value for sufficient support shrinkage, the linear shrinkage of the support has to be tuned for each case.

Fig. 6 shows the sintering curves of the commercial 8YSZ electrolyte, the in-house produced 8YSZ electrolyte and the NiO–YSZ anode materials pre-sintered at different temperatures. From Fig. 6 it can be seen that the temperature at which shrinkage starts is 1000 °C both for the commercial 8YSZ and the in-house produced nanopowder. The shrinkage behaviour of the anode material can be tailored to match that of the electrolyte by adjusting the pre-sintering temperature of the anode as shown in Fig. 6. The total relative shrinkage of the commercial 8YSZ was almost the same as for the anode substrate pre-sintered at 1000 °C. The final shrinkage of the in-house produced nanoparticle-based 8YSZ was slightly larger than that of the anode pre-sintered at 1000 °C. The values of the total shrinkage of the commercial 8YSZ powder, 8YSZ nanopowder and the anode substrates pre-sintered at different temperatures obtained from Fig. 6 are summarized in Table 2. As demonstrated below, anode shrinkage above 20% was found to be sufficient to achieve densification of the 8YSZ electrolyte film. If not otherwise noted the anode substrates used for deposition in the further discussion have been pre-sintered at 1000 °C.

Table 2
The relative shrinkage of the 8YSZ samples and the anode substrates as a function of pre-sintering temperature.

	Pre-sintering temperature (°C)				
	0	1000	1100	1200	1300
NiO–YSZ (%)	–	23	21	18	9
8YSZ commercial (%)	23				
8YSZ nanopowder (%)	26				

3.3. Dip-coating of the electrolyte layers

In order to achieve fully densified electrolyte films well-dispersed suspensions are needed. Recent results in studies by Zhitomirsky and Petric indicate that ethanol–PE–PVB is an effective solvent–dispersant–binder system for EPD of ceramic materials [11,12]. PE is an effective electrostatic and steric stabilizer. PVB is a widely used polymer and binder in ceramic processes such as tape casting [27] and dip-coating [17,20]. It also serves as an effective dispersant [34–36]. In this work, the solvent–dispersant–binder system presented by Zhitomirsky and Petric was applied to prepare suspensions for dip-coating.

In the case of the commercial 8YSZ powder, the added amounts for dispersant and binder were 0.15 g and 0.3 g, respectively [11,12]. In the case of the in-house produced 8YSZ nanopowder the amount of dispersant in the suspension was kept the same as in the case of the commercial powder. To avoid cracking of the green film during drying, the addition of different amounts of binder was studied.

In the case of the commercial YSZ powder, crack-free green films were obtained after drying. In the case of the in-house produced nanopowder, binder addition of 0.8 g to the ball-milled suspension while keeping the amount of dispersant at 0.15 g resulted in crack-free green deposits after solvent evaporation.

Deposition was obtained on all the anode substrates pre-sintered at different temperatures. However, due to the reduced porosity of the anode samples at higher pre-sintering temperatures, the wetting properties of the anode substrates to the 8YSZ suspension tended to decrease by increasing pre-sintering temperature of the anode [17].

The dried green films contain the ceramic 8YSZ particles, PE dispersant in a PVB polymer binder network and some solvent residues. The organic additives used in the manufacturing process need to be burned out prior to sintering in order to achieve the final electrolyte film. Since the organic additives decompose at much lower temperatures than that at which the 8YSZ particles sinter and in decomposing they produce big volumes of gas this has to be taken into consideration when designing the sintering program. Thiele and Setter found that PE compounds volatilize well below 900 °C [37]. A detailed description of the thermal decomposition processes for PVB can be found in the work of Masia et al. [38]. It was found that, in the presence of zirconia, PVB decomposition is to a great

extent finished at 500 °C and the remaining carbon residue elimination takes place above 800 °C. According to the sintering curves (Section 3.2) the 8YSZ starts to sinter at 1000 °C. Below this temperature the ceramic particles form a loose particle network allowing the gaseous species to freely diffuse. In this work, the sintering program applied had a slow heating rate and a heating plateau at 600 °C for 1 h (see Section 2.3) in order to remove the organic material from the green ceramic body in a controlled manner.

Further optimization and modelling of the dip-coating process, such as varying the withdrawal rate and modelling the deposition of the particles, including the effect of the meniscus, has not been undertaken yet. This will be addressed in future work.

3.4. Microstructural characterization of the final, sintered 8YSZ films

Fig. 7 shows a picture of an 8YSZ film obtained from nanopowder suspension. In the case depicted, the suspension was prepared under the same conditions as for the commercial YSZ suspension. The nanoparticles were highly agglomerated which resulted in a poorly sintered microstructure. In contrast, the commercial 8YSZ suspension exhibited better dispersion which lead to a fully dense sintered film. Fig. 8(a) shows the SEM image of commercial 8YSZ film and (b) sample cross-section, respectively. The commercial particles were sintered to grains of the size of some microns and these gains formed a well densified electrolyte film. The cross-section image shows a ~12 μm thick film with some isolated pores.

In order to improve the quality of the nanoparticle-based films, a ball-milling step was applied to break the agglomerates and to obtain larger densities of the green nanoparticle compacts. Fig. 9 shows an SEM image of an 8YSZ film obtained from nanopowder suspension subjected to ball-milling for 48 h, the amount of dispersant and binder being 0.15 g and 0.8 g, respectively. The effect of introducing the ball-milling step is clearly visible in the improved microstructure of the obtained film. However, remaining agglomerates resulted in a rough surface with voids and pin-holes.

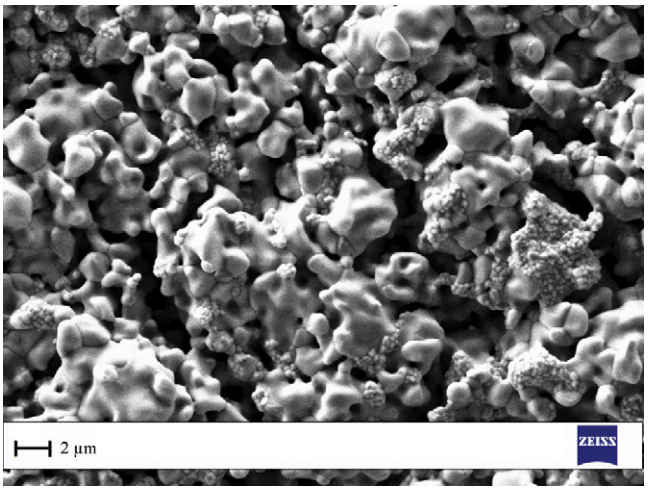

Fig. 7. SEM image of an 8YSZ film prepared from nanoparticles sintered at 1400 °C for 2 h. The amount of dispersant and binder being 0.15 g and 0.3 g, respectively.

In order to remove the bigger agglomerates suspensions obtained by ball-milling were allowed to settle for 24 h before the dip-coating process started hence depositing only the finer particles. A dramatic difference in terms of improved packing of the particles manifested itself by the formation of transparent and shiny electrolyte films after sintering. Fig. 10(a) presents an SEM image of an 8YSZ film obtained from nanopowder suspension after settling. Fig. 10(b) shows the film cross-section. The amount of organic additives in this case were 0.15 g and 0.8 g of dispersant and binder, respectively. The removal of big agglomerates resulted in smooth and uniform electrolyte microstructure. The obtained film thickness was about 12 μm.

The difference in the dispersability of the commercial 8YSZ powder and the 8YSZ nanopowder can be explained by the particle size and specific surface area. Particles naturally form agglomerates in order to reduce the surface area. The degree of agglomeration affects the dispersability and can be correlated with increasing attraction between particles with decreasing particle size [30]. According to manufacturer specifications the average particle size and specific surface area for the

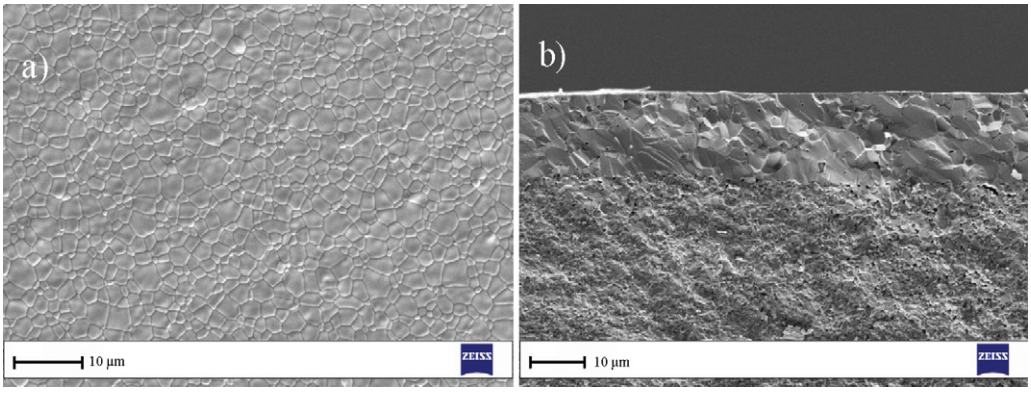

Fig. 8. SEM image of a commercial 8YSZ film (a) surface and (b) cross-section sintered at 1400 °C for 2 h. The amount of dispersant and binder being 0.15 g and 0.3 g, respectively.

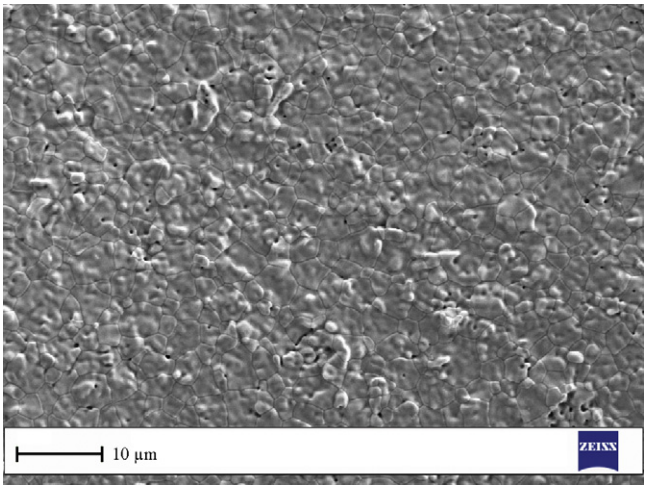

Fig. 9. SEM image of an 8YSZ film prepared from nanoparticles after ball-milling step sintered at 1400 °C for 2 h. The amount of dispersant and binder being 0.15 g and 0.8 g, respectively.

commercial powder are 230 nm and 12 $m^2\ g^{-1}$, respectively (see also Fig. 4). The particle size and the specific surface area for the nanopowder are 40 nm and 25 $m^2\ g^{-1}$, respectively. The poor densification of the nanoparticle-based electrolyte film, presented in Fig. 7, is due to the higher degree of agglomeration of the 8YSZ nanopowder caused by the smaller particle size and the larger surface area (see also [6]).

In addition to dispersability, the surface area of a powder is also the most important parameter in determining its interaction with organic additives [27]. By introducing the additional ball-milling step, the agglomerated nanopowder was ground to smaller particles. As a result more binder needed to be added to prevent the green film from cracking during drying. The amount of phosphate ester dispersant was intentionally not increased.

Phosphorus-containing dispersants for ceramic materials may give rise to some problems. In the literature, phosphorus has been known to affect the sintering properties of the material by liquid-phase sintering [39]. Also, the electrochemical properties of SOFC components have been reported to be affected by introducing phosphorus during cell operation [40,41].

A discussion of the suitability to use PE as a dispersant and the risks of PE intercalation in deposits obtained by EPD method can be found in the work by Zhitomirsky and Petric [12]. They noted that PE has been found to leave residues in ceramics obtained by tape casting. However, their experimental results indicate that the amount of dispersant needed to stabilize suspensions for EPD is much lower than the amount needed to stabilize slurries for tape casting process. In addition, only the PE molecules adsorbed onto the deposited particles are present in the obtained ceramic film. The risk of residual phosphorus in the final ceramic deposits is therefore low and PE was suggested by them to find increasing application in EPD. In this work, the amount of PE used to stabilize the suspensions for dip-coating was taken over from Zhitomirsky and Petric. It is also important to note that dip-coating is similar to EPD in the sense that only some of the total amount of added dispersant will be present in the deposited film. It is therefore suggested that PE is a suitable dispersant for dip-coating, too.

A high content of organic material in a deposited film may create problems during sintering in other ways as well. As discussed in the work by Gaudon et al. the decomposition of organic additives can lead to crack formation in the film [15]. For the reasons given in this and in the previous paragraphs further work will be done to optimize the bath composition for the nanopowder suspension.

The preparation condition of the anode was found to be important for the obtained electrolyte microstructure. Fig. 11 presents the microstructure of three deposited 8YSZ layers obtained from nanopowder suspension after settling on anode substrates pre-sintered at different temperature (a) 1100 °C, (b) 1200 °C and (c) 1300 °C. The microstructural observations revealed the effect of the pre-sintering temperature of the anode support i.e. the effect of linear shrinkage of the anode during the co-sintering process on the densification of the electrolyte film. The densification of the electrolyte film was improved by lowering the pre-sintering temperature of the anode support and hence increasing the linear shrinkage. Linear shrinkage of above 20% resulted in fully dense 8YSZ thin films in both the cases of the nanopowder and the commercial powder.

It was found through the microstructural studies of the obtained films that agglomeration of the nanoparticles was

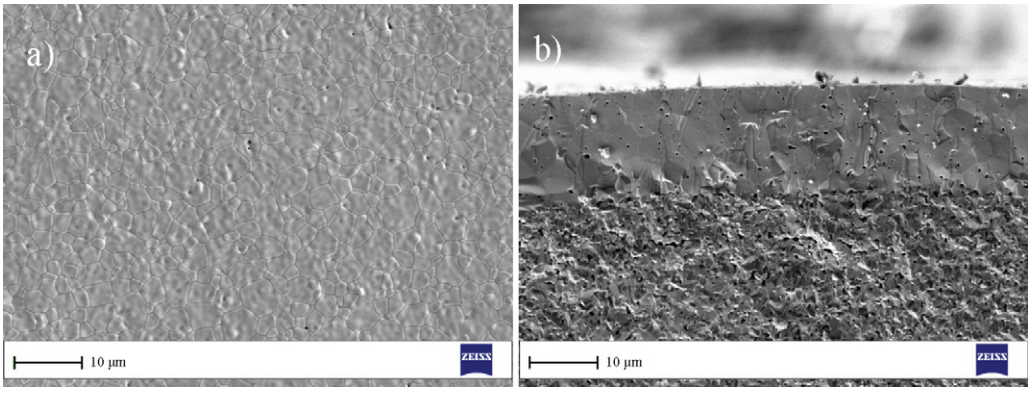

Fig. 10. SEM image of an 8YSZ film (a) surface and (b) cross-section prepared from nanoparticles sintered at 1400 °C for 2 h. The suspension was subjected to ball-milling and allowed to settle for 24 h before deposition. The amount of dispersant and binder being 0.15 g and 0.8 g, respectively.

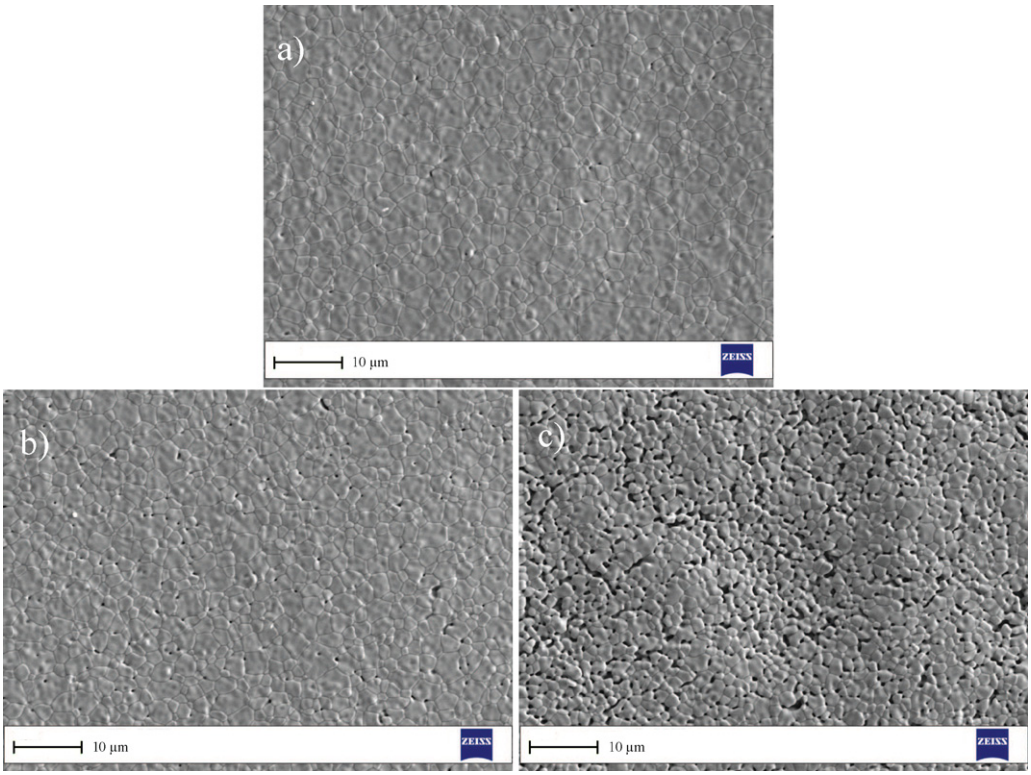

Fig. 11. SEM image of a sintered 8YSZ film prepared from nanopowder suspension after settling on anode substrate pre-sintered at (a) 1100 °C, (b) 1200 °C and (c) 1300 °C for 2 h. The amount of dispersant and binder being 0.15 g and 0.8 g, respectively.

severe. This work concentrated therefore on improving the packing of nanoparticles in the ceramic deposit to obtain smooth microstructure of the sintered film. The expected reduction in the sintering temperature of the electrolyte film by using nanopowder precursors was not observed in this study.

4. Conclusions

In this study, the microstructural features of the deposited films of 8YSZ nanopowder and commercial 8YSZ powder obtained by dip-coating on anode substrates were investigated. The effect of the suspension preparation conditions on the obtained film quality have been identified and demonstrated. The commercial 8YSZ powder exhibited better dispersability than the 8YSZ nanopowder. The difference in the dispersability was related to the difference in the particle size and specific surface area between the two powders. A procedure has been developed to improve the quality of the films obtained from nanopowder suspension. An additional ball-milling step was introduced in order to break the formed agglomerates. Crack-free green films were obtained after drying from ball-milled nanopowders suspensions by increasing the amount of binder. By allowing the suspension to settle for 24 h hence removing the bigger agglomerates, a smooth and uniform film surface was obtained.

The advantages of tuning the linear shrinkage of the anode substrate by pre-sintering conditions have been demonstrated. Deposition was obtained on all the anode substrates prepared at different pre-sintering temperatures. However, microstructural investigations revealed that anode support shrinkage of above 20% was sufficient to produce a fully densified electrolyte microstructure.

Acknowledgement

The authors wish to acknowledge the NFR (Norwegian Research Council) for funding this project. Also, the authors are grateful to Senior Engineer Egil Erichsen and Senior Research Engineer Irene Heggstad (The Electron Microscopy Laboratory, University of Bergen) for help using the TEM and SEM. In addition, the authors wish to acknowledge PhD Eugen Dorolti (Babes-Bolyai University, Physics Faculty, Romania) for performing the XRD measurements on the 8YSZ powder.

References

[1] S.C. Singhal, K. Kendall, High Temperature Solid Oxide Fuel Cells: Fundamentals, Design and Applications, first ed., Elsevier Ltd, 2003.
[2] S.P.S. Badwal, Zirconia-based solid electrolytes – microstructure, stability and ionic-conductivity, Solid State Ionics 52 (1992) 23.
[3] A.J Feighery, J.T.S. Irvine, Effect of alumina addition upon electrical properties of 8 mol% yttria-stabilised zirconia, Solid State Ionics 121 (1999) 209.
[4] T. Ishihara, K. Shimose, T. Kudo, H. Nishiguchi, T. Akbay, Y. Takita, Preparation of yttria-stabilized zirconia thin films on strontium-doped $LaMnO_3$ cathode substrates via electrophoretic deposition for solid oxide fuel cells, Journal of the American Ceramic Society 83 (2000) 1921–1927.
[5] K. Yang, J.-H. Shen, K.-Y. Yang, I.-M. Hung, K.-Z. Fung, M.-C. Wang, Characterization of the yttria-stabilized zirconia thin film electrophoretic

deposited on $La_{0.8}Sr_{0.2}MnO_3$ substrate, Journal of Alloys and Compounds 436 (2007) 351–357.
[6] Y.-H. Lee, C.-W. Kuo, C.-J. Shih, I.-M. Hung, K.-Z. Fung, S.-B. Wen, M.-C. Wang, Characterization on the electrophoretic deposition of the 8 mol% yttria-stabilized zirconia nanocrystallites prepared by sol–gel process, Materials Science and Engineering A 445–446 (2007) 347–354.
[7] S.M. Kim, J.W. Son, K.R. Lee, H. Kim, H.R. Kim, H.R. Lee, J.H. Lee, Substrate effect on the electrical properties of sputtered YSZ thin films for co-planar SOFC applications, Journal of Electroceramics 23 (2010) 153–160.
[8] P. Amezaga-Madrid, W. Antunez-Flores, J. Gonzalez-Hernandez, J. Saenz-Hernandez, K. Campos-Venegas, O. Solis-Canto, C. Ornelas-Gutierrez, O. Vega-Becerra, R. Martinez-Sanchez, M. Miki-Yoshida, Microstructural properties of multi-nano-layered YSZ thin films, Journal of Alloys and Compounds 495 (2010) 629–633.
[9] D. Waldbillig, O. Kesler, The effect of solids and dispersant loadings on the suspension viscosities and deposition rates of suspension plasma sprayed YSZ coatings, Surface and Coatings Technology 203 (2009) 2098–2101.
[10] Z. Xu, G. Rajaham, J. Sankar, D. Pai, Electrophoretic deposition of YSZ electrolyte coatings for solid oxide fuel cells, Surface and Coating Technology 201 (2006) 4484–4488.
[11] I. Zhitomirsky, A. Petric, Electrophoretic deposition of ceramic materials for fuel cell application, Journal of the European Ceramic Society 20 (2000) 2055–2061.
[12] I. Zhitomirsky, A. Petric, Electrophoretic deposition of electrolyte materials for solid oxide fuel cells, Journal of Material Science 39 (2004) 825–831.
[13] C. Xia, S. Zha, W. Yang, R. Peng, D. Peng, G. Meng, Preparation of yttria stabilized zirconia membranes on porous substrates by a dip-coating process, Solid State Ionics 133 (2000) 287–294.
[14] Y. Zhang, J. Gao, D. Peng, M. Guangyao, X. Liu, Dip-coating thin yttria-stabilized zirconia films for solid oxide fuel cell application, Ceramics International 30 (2004) 1049–1063.
[15] M. Gaudon, C. Laberty-Robert, F. Ansart, P. Stevens, Thick YSZ films prepared via a modified sol–gel route: thickness control (8–80 μm), Journal of the European Ceramic Society 26 (2006) 3153–3160.
[16] S.D. Kim, J.J. Lee, H. Moon, S.H. Hyun, J. Moon, J. Kim, H.W. Lee, Effects of anode and electrolyte microstructures on performance of solid oxide fuel cells, Journal of Power Sources 169 (2007) 265–270.
[17] T. Yamaguchi, T. Suzuki, S. Shimizu, Y. Fujishiro, M. Awano, Examination of wet coating and co-sintering technologies for micro-SOFCs fabrication, Journal of Membrane Science 300 (2007) 45–50.
[18] R.Z. Liu, S.R. Wang, B. Huang, C.H. Zhao, J.L. Li, Z.R. Wang, Z.Y. Wen, T.L. Wen, Dip-coating and co-sintering technologies for fabricating tubular solid oxide fuel cells, Journal of Solid State Electrochemistry 13 (2009) 1905–1911.
[19] L. Zhang, H.Q. He, W.R. Kwek, J. Ma, E.H. Tang, S.P. Jiang, Fabrication and characterization of anode-supported tubular solid-oxide fuel cells by slip casting and dip coating techniques, Journal of the American Ceramic Society 92 (2009) 302–310.
[20] Z. Wang, K. Sun, S. Shen, X. Zhou, J. Qiao, N. Zhang, Effect of co-sintering temperature on the performance of SOFC with YSZ electrolyte thin films fabricated by dip-coating method, Journal of Solid State Electrochemistry 14 (2010) 637–642.
[21] J.-J. Lee, H. Moon, H.-G. Park, D.I. Yoon, S.-H. Hyun, Applications of nano-composite materails for improving the performance of anode-supported electrolytes of SOFCs, International Journal of Hydrogen Energy 35 (2010) 738–744.
[22] V. Gil, J. Gurauskis, R. Campana, R.I. Merino, A. Larrea, V.M. Orera, Anode-supported microtubular cells fabricated with gadolinia-doped ceria, Journal of Power Sources 196 (2011) 1184–1190.
[23] R.M. German, Sintering Theory and Practice, first ed., John Wiley & Sons, 1996.
[24] O. Vasylkiv, Y. Sakka, Synthesis and colloidal processing of zirconia nanopowder, Journal of the American Ceramic Society 84 (2001) 2489–2494.
[25] M.F. Han, X.L. Tang, H.Y. Yin, S.P. Peng, Fabrication, microstructure and properties of a YSZ electrolyte for SOFC, Journal of Power Sources 165 (2007) 757–763.
[26] P Sarkar, D. De, H. Rho, Synthesis and microstructural manipulation of ceramics by electrophoretic deposition, Journal of Materials Science 39 (2004) 819–823.
[27] R.E. Mistler, E.R. Twiname, Tape Casting-Theory And Practice, first ed., The American Ceramic Society, Ohio, US, 2000.
[28] J. Will, M.K.M. Hruschka, L. Gubler, L.J. Gauckler, Electrophoretic deposition of zirconia on porous anodic substrates, Journal of American Ceramic Society 84 (2001) 328–332.
[29] T. Hosomi, M. Matsuda, M. Miyake, Electrophoretic deposition for fabrication of YSZ electrolyte film on non-conducting porous NiO–YSZ composite substrate for intermediate temperature SOFC, Journal of the European Ceramic Society 27 (2007) 173–178.
[30] H. Ferkel, R.J. Hellming, Effect of nanopowder agglomeration on the densities of nanocrystalline ceramic green bodies and their sintering behaviour, Nanostructured Materials 11 (1999) 617–622.
[31] D. Maeland, C. Suciu, I. Waernhus, A.C. Hoffmann, Sintering of 4YSZ (ZrO^{2+} 4 mol% Y_2O_3) nanoceramics for fuel cells (SOFCs), their structure and conductivity, Journal of the European Ceramic Society 29 (2009) 2537–2547.
[32] C. Suciu, A.C. Hoffmann, P. Kosinski, Obtaining YSZ nanoparticles by sol–gel method with sucrose and pectin, Journal of Materials Processing Technology 202 (2008 a) 316–320.
[33] C. Suciu, A.C. Hoffmann, A. Vik, F. Goga, Effect on process parameters on YSZ nanoparticles obtained by modified sol–gel route, Chemical Engineering Journal 138 (2008 b) 608–615.
[34] S. Bhattacharjee, M.K. Paria, H.S. Maiti, Polyvinyl butyral as a dispersant for barium titanate in non-aqueous suspension, Journal of Materials Science 28 (1993) 6490–6495.
[35] J.-H. Jean, S.-H. Yeh, C.-J. Chen, Adsorption of polyvinyl butyral in non-aqueous ferrite suspension, Journal of Materials Reseach 12 (1997) 1062-.
[36] A. Mukherjee, R. Khan, B. Bera, H.S. Maiti, I: Dispersability of robust alumina particles in non-aqueous solution, Ceramics International 34 (2008) 523–529.
[37] E. Thiele, N. Setter, Lead zirconate titanate particle dispersion in thick-film ink formulations, Journal of the American Ceramic Society 83 (2000) 1407–1412.
[38] S. Masia, P.D. Calvert, W.E. Rhine, H.K. Bowen, Effect of oxide on binder burnout during ceramic processing, Journal of Materials Science 24 (1989) 1907–1912.
[39] D.Y. Gao, R.S. Guo, Densification and properties of barium zirconate ceramics by addition of P_2O_5, Materials Letters 65 (2010) 573–575.
[40] M.J. Zhi, X.Q. Chen, H. Finklea, I. Celik, N.Q.Q. Wu, Electrochemical and structural analysis of nickel–yttria-stabilized zirconia electrode operated in phosphorus-containing syngas, Journal of Power Sources 183 (2008) 485–490.
[41] W. Liu, X. Sun, L.R. Pederson, O.A. Marina, M.A. Khaleel, Effect of nickel–phosphorus interactions on structural integrity of anode-supported solid oxide fuel cells, Journal of Power Sources 195 (2010) 7140–7145.